IJCRT.ORG ISSN : 2320-2882

INTERNATIONAL JOURNAL OF CREATIVE RESEARCH THOUGHTS (IJCRT)

An International Open Access, Peer-reviewed, Refereed Journal

Effective As(V) removal from aqueous solution by novel iron-oxide-biochar composites derived from chemical-carbonization of flax plant waste: Performance, kinetics, and mechanisms

Naincy Sahu*, Siddhartha Shukla, Vinod Kumar Chaudhary, Saurabh Kumar, Naveen Patel, Brijesh Kumar Yadav

Department of Environmental Science, Dr. Rammanohar Lohia Avadh University, Ayodhya-224001, Uttar Pradesh, India

Graphical abstract

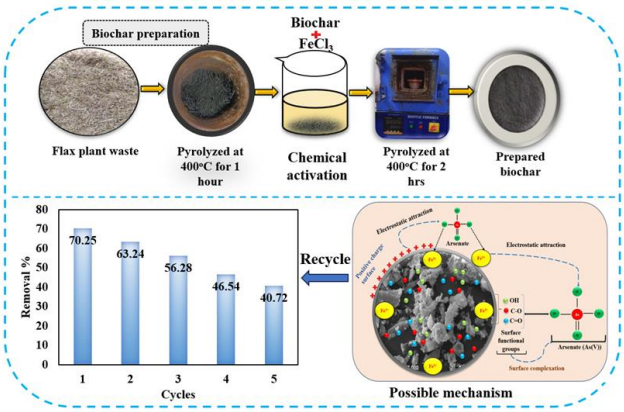

Abstract

This study focuses on the utilization of a novel waste-derived material for biochar synthesis. Dried flax plant waste was used as the precursor to produce biochar, named as FPBC. The synthesized biochar was subsequently modified using $FeCl_3$, resulting in an iron-enhanced biochar referred to as FeFPBC. The prepared material was then employed as an adsorbent for the removal of Arsenic (As(V)) from aqueous solutions. The synthesized biochar was characterized by using Fourier-transform infrared spectroscopy (FTIR), Scanning Electron Microscopy (SEM), Energy Dispersive X-ray Spectroscopy (EDS) and pH_{ZPC}. The removal of As(V) from aqueous solutions carried out with FeFPBC by batch study. The regeneration experiments data revealed that synthesized biochar can be regenerated and reused four times with efficient removal percent of As(V). Adsorption isotherm, kinetic and thermodynamic studies were analyzed for As(V) uptake on the surface of prepared biochar (FeFPBC). As(V) adsorption on the biochar accepted Freundlich-model ($R^2 = 0.9921$) and Pseudo-second-order kinetics-model ($R^2 = 0.9934$). In the thermodynamics study it

was found that the adsorption process was exothermic in nature. The FeFPBC was obtained effective adsorbent. The maximal As(V) uptake removal was achieved 78.87 % at neutral pH and ambient temperature.

Keyword: Biochar; Adsorption; Arsenate ion; Flax Plant; Batch study

1. Introduction

The rapid growth of agricultural practices in agrarian economies has significantly increased the generation of agricultural residues, transforming them into a major source of environmental pollution (Maji et al., 2020). The combustion of straw and the improper disposal of livestock droppings have created various environmental issues. The direct burning and unregulated waste disposal significantly endanger rural ecosystems and degrade the quality of farmers lifestyle (Rathod et al., 2024). The improper disposal of agricultural waste causes environmental pollution, as well as leads to loss of potential bioenergy resources. The recycling and repurposing of agricultural waste are effective ways for environmental conservation, energy infrastructure, and agricultural progress (Peng et al., 2023). Flax plant waste is a common agricultural waste produced during flax seed processing. Due to its high content of cellulose, hemicellulose, and lignin, it serves as a promising raw material for biochar production (Mukhambet et al., 2022). Through pyrolysis under limited oxygen conditions, a biochar with a porous structure, high carbon content, and good adsorption properties can be obtained from flax plant waste. The resulting biochar has potential applications in soil improvement, carbon sequestration, wastewater treatment, and environmental remediation (Dong et al., 2026). Utilizing flax plant waste for biochar production not only adds value to agricultural waste but also contributes circular bioeconomy practices. Arsenic is a carcinogenic element which creates human health risk and causes major threat to environment (Muzaffar et al., 2023). Arsenic is the twentieth highest natural metalloid present in the earth's crust. Arsenic contamination of water is a major environmental concern (Genchi et al., 2022). Arsenic (As) is a toxic element found in the environment, causing significant risks for human and ecosystems. The permissible limit of arsenic in groundwater has been set at 10 µg/L (Sahu et al., 2022). Human activities are the main cause of environmental pollution. Pollution exposes thousands of people to serious health risks through polluted food and water, as well as the use of polluted water for irrigation (Rahidul (2022)). These pollutants may enter water bodies through natural processes, such as the dissolution of minerals from the Earth's crust, and through anthropogenic activities, including industrial discharges and fossils (Khan and Flora, 2023). Trivalent arsenic As(III) is considered 60% more toxic than pentavalent arsenic As(V) due to its high reactivity with the phosphate group (Majumder et al., 2023). As contamination has been identified as a global issue, affecting regions including Southeast Asian countries such as India and Bangladesh (Natasha et al., 2019). Particularly, in India, arsenic (As) contamination has been detected in the groundwater in West Bengal, Odissa, Chhattisgarh, Uttar Pradesh and other states (Marghade et al., 2023). To mitigate the concentration of As ions in ground water and wastewater, various treatment methods can be employed. These include ion exchange, precipitation, coagulation, reverse osmosis, membrane filtration, and adsorption (Kudu and Naskar (2021)). Out of these, adsorption is frequently preferred due to its advantages, such as cost-effectiveness, operational simplicity, minimal chemical requirements, and rapid processing (Rashid et al. in 2021). Several adsorbents such as fly ash, natural materials, carbon rich materials, biochar, nanoparticles, iron coated absorbent, etc. were utilized for As removal from aqueous solution (Verma et al., 2022).

2. Materials and chemical

Flax plant agricultural residue was collected from agricultural areas near Ambedkar Nagar, Uttar Pradesh, India. All chemicals and reagents used in this study were of analytical grade, including sodium arsenate, hydrochloric acid, sodium hydroxide, potassium iodate, antimony potassium tartrate, ammonium molybdate, sulphuric acid, L-ascorbic acid, and anhydrous ferric chloride, which were purchased from Thermo Scientific, India.

2.1. Biochar preparation

In this study, collected flax plant waste was used for synthesis of biochar as per the method explained by Wen et al., (2021) with some modifications (**Fig.1**). Flax plant waste was initially cleaned and thoroughly rinsed using double-distilled water at least three to four times. It was then kept in an oven at 60ºC for drying before it's grounded. The dried and ground flax plant waste was subjected to pyrolysis in a muffle furnace at 400 °C for 1 hour, yielding the raw biochar (FPBC). After heat treatment, the sample was cooled. The prepared raw-biochar (FPBC) was then washed multiple times, dried, and kept in a container for future utilization. The obtained FPBC was modified with ferric chloride solution by adding raw-biochar into the $FeCl_3.6H_2O$ solution at a 20:1 ratio (FPBC: ferric chloride). The prepared mixture was stirred and placed into oven at 60 ºC for one hour. Then the mixture was pyrolyzed again at 400 ºC for two hours for better Fe loading and binding with FPBC. The synthesized sample was washed, dried, crushed and placed into airtight bottle for further applications. The obtained iron modified FPBC named as FeFPBC.

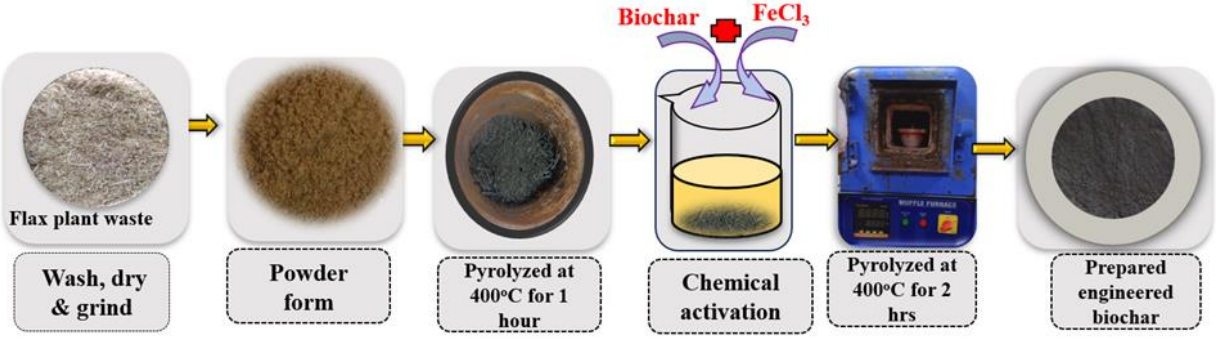

Fig.1. Pictorial representation of biochar synthesis

2.2. Characterization of FeFPBC

The Scanning Electron Microscopy (SEM) and Energy Dispersive X-ray Spectroscopy (EDS) methods were used for the examination of biochar's surface morphological structure and elemental composition. These tests were conducted using the JEOL-6490 LV model from Japan. The availability of the FeFPBC were confirmed by using instrument FTIR (Fourier transform infrared spectrometer, model no: Nicole 6700; Thermo-Scientific, USA). The crystalline structure of the FeFPBC was analyzed using X-ray diffractometer (XRD: PANalytical X'Pert Pro, Netherlands). For the analysis of pH_{ZPC}, initially 0.2g of the adsorbent were added into 20ml of a 0.01M NaCl solution. After that, the pHzpc of the FeFPBC was estimated. The pH levels were adjusted from 2 to 10 using 0.1M solutions of sodium-hydroxide (NaOH) and hydrochloric-acid (HCl). After a duration of 48 hours, the final pH was recorded (Bhan et al., 2022).

2.3. Batch Study

Using the 250mL conical flask, the laboratory-scale batch adsorption experiment was conducted to examine the removal of As(V). The flask was filled with 50mL of As(V) solution, to which varying dosages of FeFPBC were added. The initial concentration, pH, and temperature were carefully controlled prior to the experiment. The flask was then placed in an orbital shaker and incubated at 25°C with continuous rotation at 100 rpm. After reaching equilibrium, the samples were filtered, and the residual concentration of As(V) was estimated to use a UV-VISIBLE Spectrophotometer at an absorbance wavelength of 880 nm. The efficiency of As(V) removal was then calculated using the equation Verma et al., 2019 and Bhan and Singh. (2022), given below-

$$\text{Removal } \% = \frac{C_o - C_t}{C_o} \times 100 \qquad (1)$$

$$\text{Adsorption capacity } (q_e) = \frac{C_o - C_t}{m} \times V \qquad (2)$$

Here, Co = initial As (V) concentration, Ct = remaining As (V) concentration, qe = concentration at equilibrium, m = adsorbent mass in gram, V = liquid phase volume (L).

3. Results and discussion

3.1. Characterization

3.1.1. SEM and EDS

The analysis of morphological characteristics and elemental composition of prepared biochar surfaces, before and after As(V) adsorption was detected by SEM equipped with EDS examination. Before and after As(V) adsorption demonstrated through the SEM and EDS represented in **Fig.2.** SEM image shows the biochar's surface rough and irregular in shape due to the clumping of particles. EDS results show that carbon and oxygen content were present on biochar surface. Thus, the biochar surface is carbon rich.

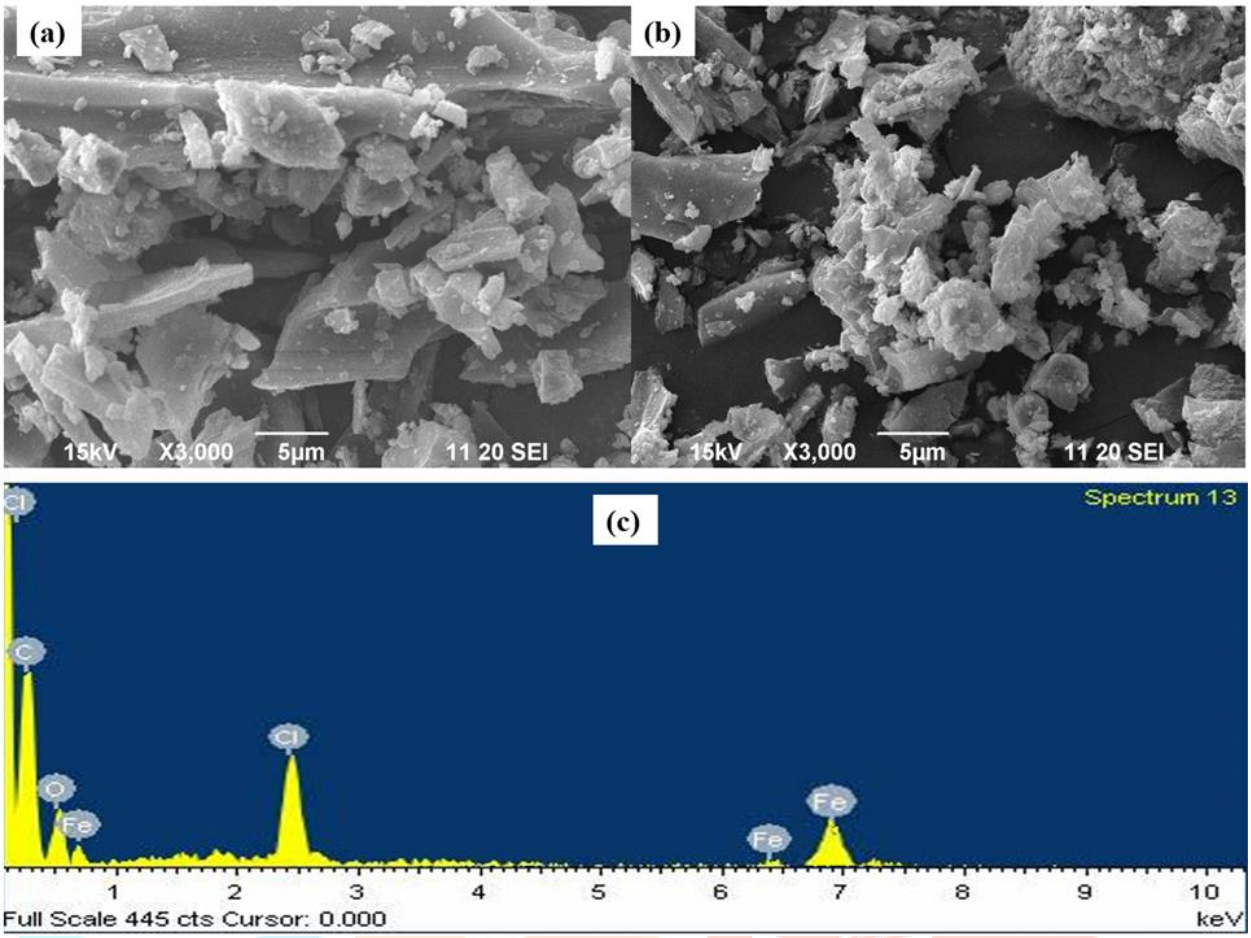

Fig. 2. SEM analysis (a) for before adsorption, (b) for after As(V) adsorption on FeFPBC.

3.1.2. FTIR

The occurrence of surface functional groups before and after adsorption were analysed by using FTIR and the obtained spectrum of FTIR are depicted in **Fig.3.a.** The small peak at 3725.98 cm^{-1} is related to the OH stretching vibration (Wu et al., 2021). The peak appeared between 400 to 800 cm^{-1} was represents to C-O group (Ibrahim et al., 2019; Rawat and Singh, (2023); Bishnoi et al., 2018). The wavenumber ranges from 1803.74 to 1679.11 cm^{-1} related to carbonyl group (C=O) (Kahmann et al., 2018). The peak at 846.32 are assigned for aromatic C–H out-of-plane bending vibrations group (Rawat and Singh, (2021). Before adsorption, the characteristic peak at 501.56 cm^{-1} shifting to 492.24 cm^{-1} after adsorption, represents the Fe-O stretching vibration due to presence of Fe_3O_4 (Bishnoi et al., 2018). Presences of Fe peak confirming the successfully binding of iron onto raw biochar surface. After As (V) adsorption, two peaks at 722.52 cm^{-1} and 501.56 cm^{-1} are shifting to 731.61 cm^{-1} and 492.24 cm^{-1}, two new peaks at 671.34 cm^{-1} and 846.32 cm^{-1} have arisen, respectively. The peak at 671.34 cm^{-1} is attribute to the asymmetrical stretching of As-OH on to the surface of FeFBC (wang et al., 2015; Sahu et al., 2021). Slight changes and presence of As-O stretching confirming the possible binding of As(V) on to the surface of FeFPBC.

3.1.3. XRD

The amorphous and crystalline structures of synthesized biochar was analysed via XRD analysis. XRD patterns of FeFPBC before and after adsorption are displayed in **Fig.3.b.** The distinct and sharp peaks were obtained for iron loaded biochar (FeFPBC), which shows the prepared FeFPBC adsorbent was crystalline in nature (Sahu et al., 2021). The distinct XRD peaks at $2\Theta = 24.29^o$, 33.15^o, 35.55^o, 40.82^o, 49.42^o, 54.14^o, and

62.27° were detected for FeFBC before and after As(V) adsorption. Additionally, the values at 24.29°, 33.15°, 35.55°, 40.82°, 49.42°, 54.14°, and 62.27° corresponds to the presence of Fe_3O_4. This suggests the successful deposition of iron oxides onto the biochar surface (Daneshvar et al., 2018; Verma et al., 2022).

3.1.4. Point-Zero-Charge (pH_{zpc})

The pH at the pH_pZC was determined to evaluate the surface characteristics of the adsorbent, representing the pH at which the net surface charge is neutral. The pH_pZC provides insight into the acidic or basic nature of the adsorbent surface and influences both the solution pH and the electrostatic interactions between the adsorbent surface and adsorbate ions during the adsorption process. The pH_{ZPC} value of FeFPBC was found to be 3.054. whereas pH_{ZPC} value was confirming that biochar surface was positively charged **(Fig.3.c).**

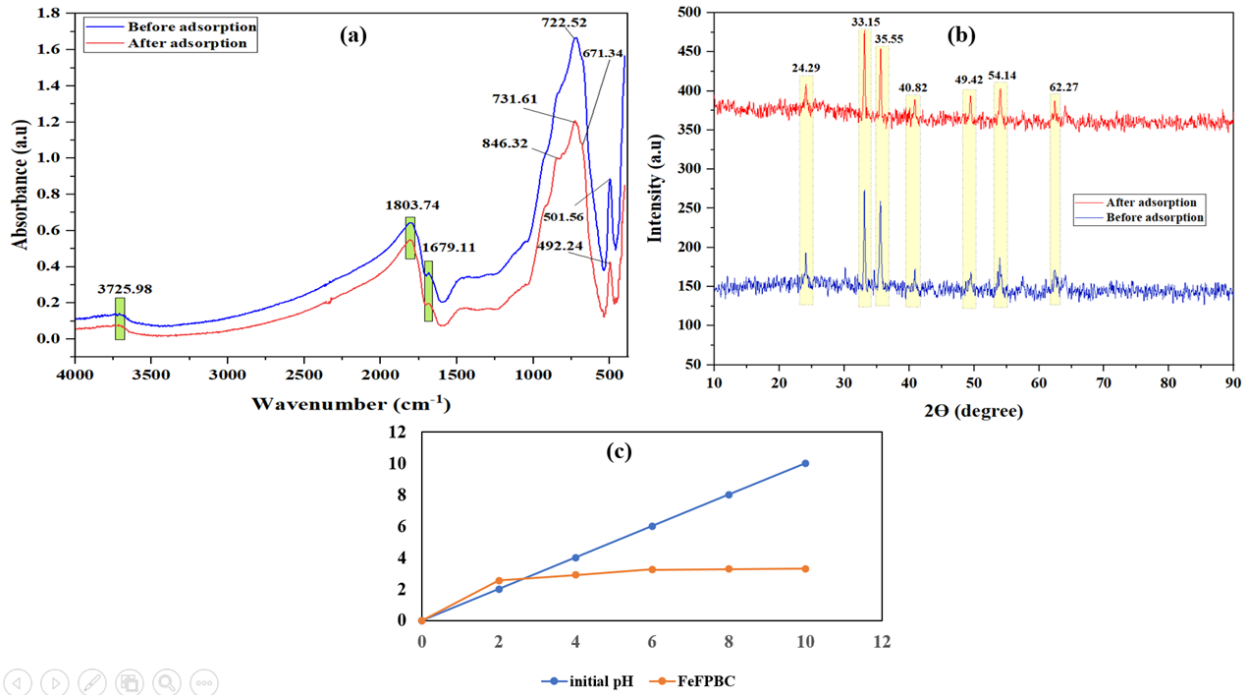

Fig.3. (a) FTIR analysis, (b) for XRD anlysis, (c) for pH_{zpc} analysis of FeFPBC.

3.2. Removal of As(V) using batch reactor

3.2.1. Effect of dose

The adsorption of As(V) using FeFPBC at different biochar dosages is presented in Fig. 4a. The effect of adsorbent dosage was evaluated by varying the FeFPBC concentration from 0.5 to 3.5 g/L under neutral pH, ambient temperature, and an starting As(V) concentration of 1 mg/L. The results showed that the highest As(V) removal efficiency (75.05%) was achieved at a dosage of 3 g/L. A further increase in biochar dosage resulted in a slight decline in adsorption efficiency, which may be attributed to particle agglomeration and reduced availability of active adsorption sites (Verma et al., 2022). Therefore, an adsorbent dosage of 3 g/L was selected for subsequent adsorption experiments.

3.2.2. Effect of pH

The solution pH is critical in determining adsorption efficiency, as it influences the surface charge of the adsorbent, the degree of adsorbate ionization, and the speciation of arsenic. The effect of solution pH on As(V) adsorption by FeFPBC was investigated over a range of 2–10 pH, and the results are presented in Fig. 4b. As(V) adsorption increased with increasing pH from 2 to 7, reaching its maximum at pH 7. Beyond this point,

the removal efficiency decreased slightly as the pH increased from 7 to 10. The maximal As(V) removal efficiency 75% was found at 7pH. The maximum adsorption was found at 6 to 7 pH. Adsorption of As(V) depends on specific As species and solution pH (Verma et al., 2019).

3.2.2. Effect of concentration

The effect of starting As(V) concentration on adsorption performance was investigated by changing the As(V) concentration from 0.5 to 2.5 mg/L. Maximum (78%) adsorption was found at 0.5mg/L initial As(V) concentration and the equilibrium occurred at 300 mins of As(V) adsorptions. As depicted in **Fig. 4.c.** the adsorption percentage decreased from 78% to 65.07% as increasing the concentration from 0.5 to 2.5. This decline may be attributed to the saturation of available adsorption sites on the biochar surface, reducing its capacity to adsorb additional As(V) ions (Siddique et al., 2020).

3.2.3. Effect of temperature

The Temperature effects on As(V) adsorption were investigated between 25°C and 55° under the optimized conditions like neutral pH, adsorbent dosage of 3 g L^{-1} and an initial As(V) concentration of 1 mg L^{-1}. As shown in **Fig. 4.d**, the highest As(V) removal efficiency (78%) was achieved at 25°C. As the adsorption process is exothermic, a gradual decline in adsorption efficiency was observed at higher temperature (Bhan et al., 2023).

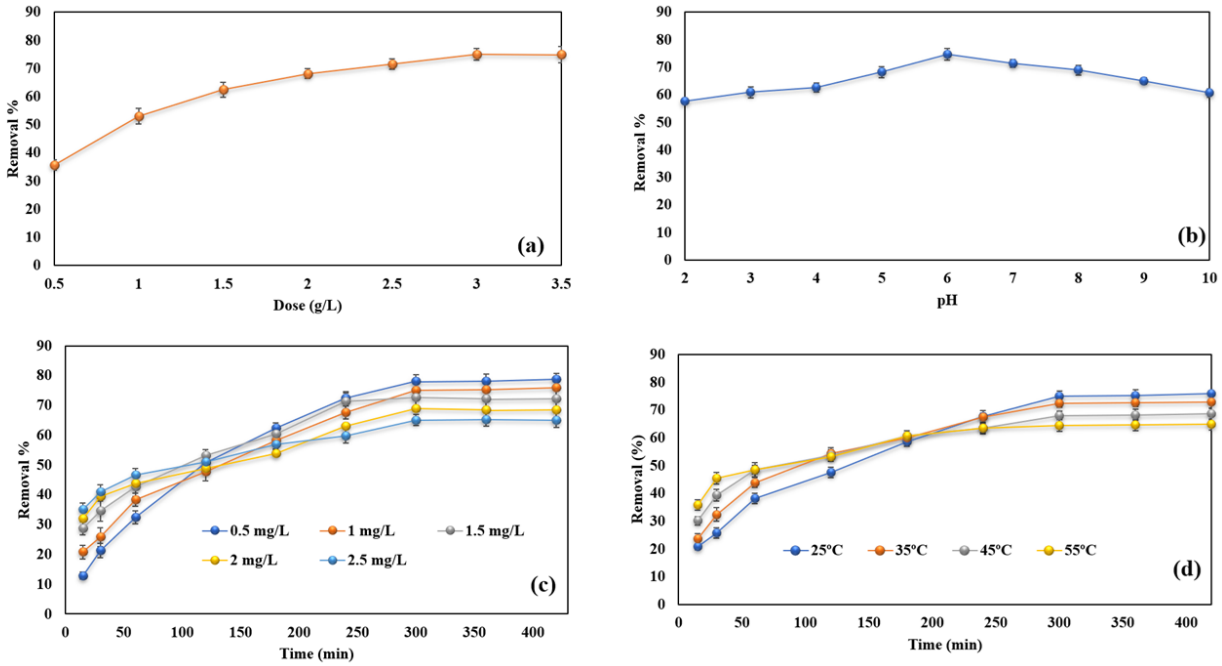

Fig.4. (a) for effect of dose, (b) for effect of pH, (c) for effect of initial As(V) concentration and contact time, (d) for effect of temperature

3.3. Adsorption isotherm models

Adsorption isotherm models were applied to investigate the relationship between the equilibrium concentration of As(V) in solution (C_e) and the adsorption capacity of FeFPBC at equilibrium (q_e). The equilibrium adsorption data were fitted using the Langmuir isotherm (LI), Freundlich isotherm (FI), and Temkin isotherm (TI) models to better understand the adsorption behavior and evaluate the adsorption mechanism of As(V) onto FeFPBC. The resulting isotherm parameters are summarized in **Table 1**.

The LI model considers that adsorbent surface is covered with the saturated monolayer of adsorbate ions. This model proposes that monolayer structure of As(V) ions take place on the homogenous adsorbent surface. There are two linear and non-linear equations given below (Eqs. (3) and Eqs. (4))

$$C_e/q_e = \frac{1}{Q_0 b} + \left(\frac{1}{Q_0}\right) C_e \quad (3)$$

$$R_L = \frac{1}{1 + bC_0} \quad (4)$$

where, C_e/q_e represented as specific adsorption against C_e (equilibrium concentration). The Langmuir constant Q_0 (mg/g) and energy constant b (L/mg) signify the maximal adsorption capacity and adsorption rate, respectively. C_0 (mg/L) represented as initial As(V) concentration. **Fig.5.a.** shows the plot and relationship between the slope and intercept. The corresponding values are listed in **Table 1.** R_L shows the behavior of adsorption process. where, the R_L indicates varying adsorption behaviors like R_L >1 (unfavorable), $0<R_L<1$ (favorable), (R_L=1) linear (Gautam et al., 2018).

The FI model considers the multilayer adsorption on a heterogeneous adsorbent surface (Vigdorowitsch et al., 2021). This model describes the relationship between the equilibrium adsorption capacity of As (q_e) and its equilibrium concentration (C_e). The linear and non-linear forms of the FI model are presented in Eq. (5).

$$\ln q_e = \ln K_F + \left(\frac{1}{n}\right) \ln C_e \quad (5)$$

Here, the concentration of As(V), adsorbed As(V) amount, and capacity of FeFPBC for As(V) uptake denoted as C_e (mg/L), q_e (mg/g), and K_f (mg/g(L/mg)$^{1/n}$). The 1/n presented as FI constant. Their values are obtained from the graph plotted between $\ln q_e$ verses $\ln C_e$ **(Fig.5.b.)** (Vigdorowitsch et al., 2021).

The TI model explains the effect of temperature using uniform distribution of binding energies across the adsorbent surface. It predicates that the adsorbate-adsorbent interactions lead to a reduction in adsorption heat. This phenomenon is due to increase in surface coverage during the adsorption process.

$$q_e = B \ln K_T + B \ln C_e \quad (6)$$

$$q_e = \frac{RT}{b} \ln K_T C_e \quad (7)$$

Where B is a constant (RT/b), R is the gas constant (8.314 J/mol K, and K_T is the TI constant (L/g) with the given heat of adsorption (J/mol). The TI constants B and K_t were determined from the slope and intercept of the q_e versus $\ln C_e$ plot, respectively. Their values are listed in **Table 1**, and the corresponding plot is shown in **Fig. 5.c** (Verma et al., 2022).

The study of these adsorption isotherm models shows that the regression coefficient (R^2) values for the LI, FI and TI model are 0.999, 0.9921 and 0.9859 respectively. It is clearly seen that with FI model the regression coefficient is slightly higher than other models. Which indicates that the Freundlich equation provided the best fit for the adsorption of As(V) on FeFPBC.

Table 1. Isotherm parameters for As(V) adsorption on FeFPBC

Langmuir Isotherm	Q_o(mg/g)	1.154734
	b(L/mg)	1.284104
	R_L	0.280253
	R^2	0.999
Freundlich Isotherm	K_F(mg/g(L/mg)1/n)	0.566998
	N	1.434103
	R_2	0.9921
Temkin Isotherm	K_T	12.85281
	B	0.2007
	R^2	0.9859

3.4. Intraparticle diffusion (IPD) model

The arbitrary or mechanical explanation of interface of the solid-liquid layer and the transfer of adsorbate to the solid adsorbent can be given by intraparticle diffusion (IPD) model. It concludes that the intercept can provide information regarding the boundary layer thickness. More amount of surface adsorption results into large value of intercept (Sahu et al., 2020a, b). The equation for the IPD model, as proposed by Weber–Morris, is as follows:

$$q_t = k_i t^{0.5} + C \qquad (8)$$

where C is a constant (mg/g) with given thickness of boundary layer and k is the rate constant in (mg/(g min0.5)) of the IPD model. **Fig.5.d** illustrates that the linear graph does not intersect the origin, confirming that IPD is not solely responsible for the rate control of As adsorption on FeFBC. The parameters of the IPD model are detailed in **Table 2**.

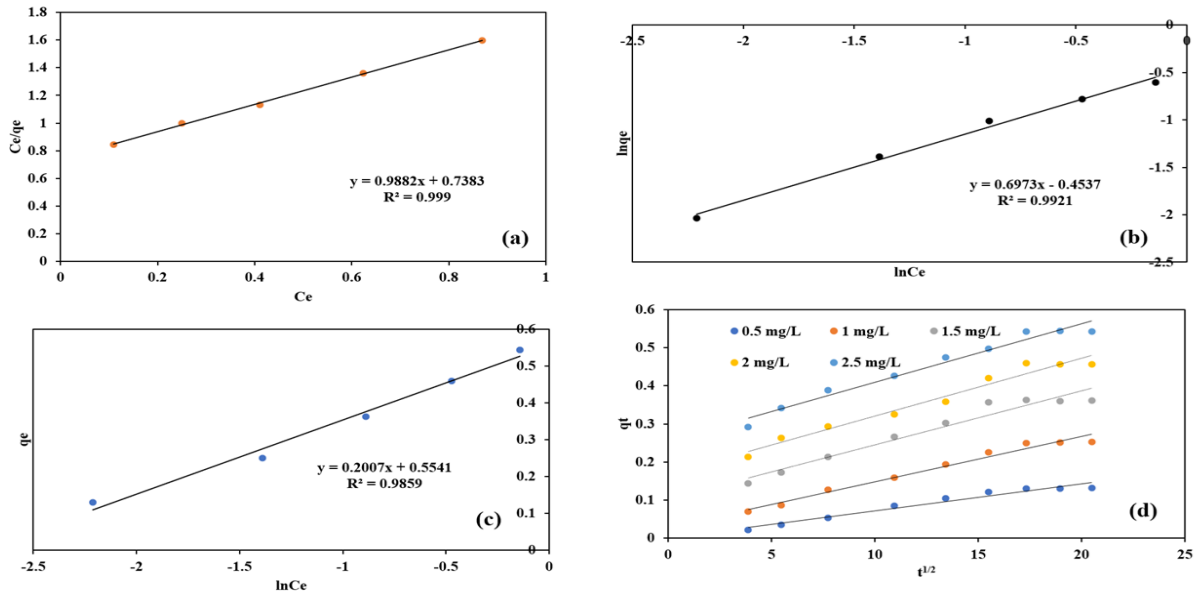

Fig.5. (a) for Langmuir isotherm, (b) for Freundlich isotherm, (c) for Temkin isotherm, (d) for intraparticle diffusion model

Table 2. Intraparticle diffusion parameters for As(V) removal on FeFPBC

C_0 (g/L)	Ki (mg g^1/min)	C (mg^{-1})	R^2
0.5	0.0071	0.0004	0.9635
1	0.0119	0.0287	0.9775
1.5	0.0142	0.1024	0.9519
2	0.0152	0.168	0.9684
2.5	0.0153	0.2561	0.9696

3.5. Adsorption kinetics

The adsorption kinetics study is essential for evaluation of adsorption interaction mechanism. It provides information of As(V) adsorption rate onto FeFPBC surface. The kinetics models Pseudo-first-order (PFO) and pseudo-second-order (PSO) were utilized for the investigation of adsorption data of As(V). The mathematical expression of PFO and PSO were presented via given below Eqs (6) and Eqs. (7), resepectively.

$$\log(q_e - q_t) = \log q_e - \left(\frac{k_1}{2.303}\right) \times t \qquad (9)$$

$$\frac{t}{q_t} = \frac{1}{k_2 q_e^{\,2}} + \left(\frac{1}{q_e}\right) \times t \qquad (10)$$

Where, q_e and q_t presented the amount of As(V) adsorption on to FeFPBC at equilibrium and time. Thus, adsorption rate constant, K_1(1/min) represented for PFO and K_2 (mg/g/min) represented PSO. The equilibrium adsorption capacities were measured via graph plotted between log(qe-qt) verses time (**Fig. 6.a,b**) and corresponding values are summarized in **Table 3**. The kinetic analysis revealed that the pseudo-second-order model provided the best fit for the adsorption data, with high correlation coefficient (R^2) values ranging from 0.9934 to 0.9955 (**Table 3**). These observations indicate that the removal of As(V) is predominantly influenced by a chemisorption mechanism involving chemical interactions between the biochar surface and the adsorbate (Elhamdy et al., 2025; Bhan et al., 2022).

Table 3. Kinetic parameters for As(V) removal on FeFPBC

Pseudo first order				**Pseudo second order**		
C_0 (mg/L)	q_e (mg/g)	$K_{1(min-1)}$	R^2	q_e (mg/g)	K_2 (g/(mg min))	R^2
0.5	0.07605	0.000174	0.0024	0.172399	0.05004	0.9934
1	0.132617	0.000174	0.0036	0.300888	0.042464	0.9862
1.5	0.123055	-0.00048	0.0418	0.403405	0.055843	0.9927
2	0.16512	0.000564	0.1194	0.497686	5.01E-05	0.9869
2.5	0.265033	0.001476	0.279	0.575341	0.063366	0.9955

3.6. Thermodynamic studies of As(V) adsorption on FeFPBC

The thermodynamic studies are done at various temperature levels like 25 ℃, 35 ℃, 45 ℃, and 55 ℃ for validation the of thermodynamic parameters. The parameters including the changes in entropy (ΔS), Gibbs free energy (ΔG), and enthalpy (ΔH) during the adsorption of As(V) on FeFPBC, were calculated using the following equations and their values are listed in **Table 4**:

$$K_c = \frac{q_e}{C_e} \quad (11)$$

$$\ln K_c = \frac{\Delta S}{R} - \frac{\Delta H}{RT} \quad (12)$$

$$\Delta G = \Delta H - T\Delta S \quad (13)$$

where Kc represents the thermodynamic constant in (L/g), R is the gas constant given by 8.314 J/mol K and T is the temperature in Kelvin. Saikia et al., 2017 presented that the relationship between enthalpy and entropy can be determined by plotting ln Kc versus 1/T. In this study, we found out that the values of the ΔH are negative, which indicates the exothermic nature of adsorption process as shown in **Table 3**. The negative values of ΔG and the positive entropy change (ΔS) indicate that the adsorption process is spontaneous and is accompanied by an increase in randomness at the FeFPBC surface (Rawat et al., 2021). The thermodynamic plot is presented in **Fig.6.c**.

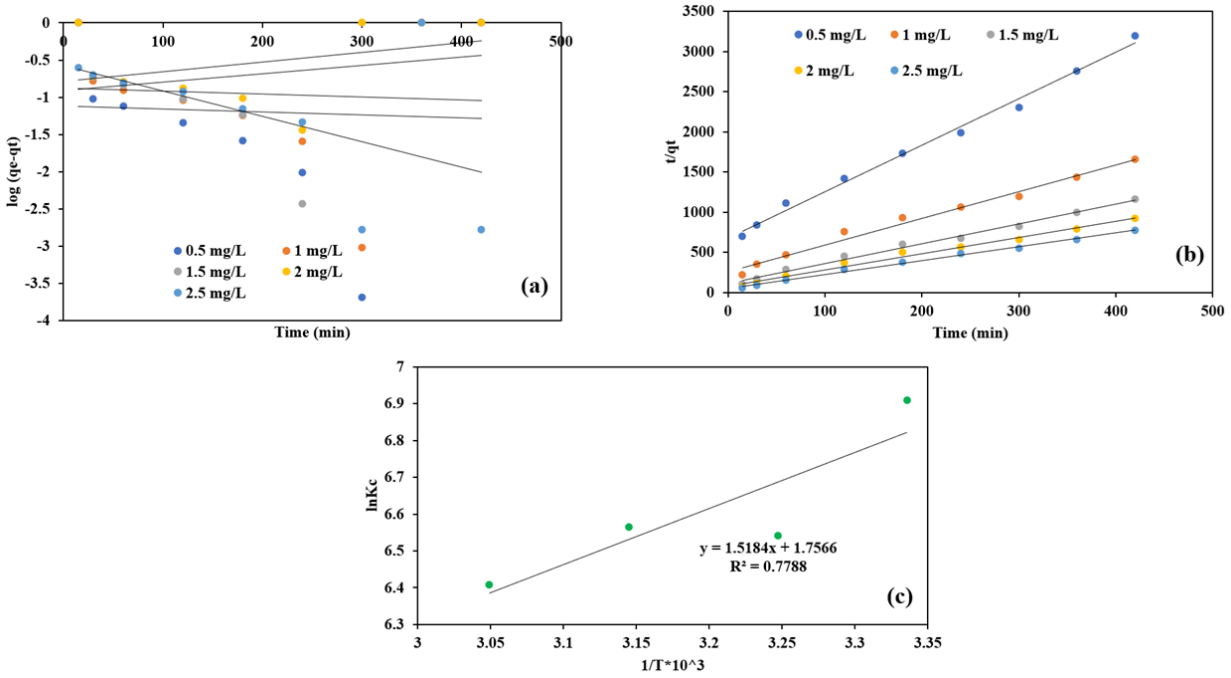

Fig.6. (a) for Pseudo-first-order, (b) for pseudo-second-order, (c) for Thermodynamic study

Table 4. Thermodynamic parameters for As(V) removal

parameters	Temperature (K)	
ΔG°(KJ/mol)	298	-4364.73
	308	-451077
	318	-4656.81
	328	-4802.86
ΔH (J/mol)		-12.624
ΔS (J/mol K)		14.60437

3.7. Proposed mechanism for adsorption of As(V)

Adsorption of As(V) on biochar is governed by various mechanisms. There are two most important mechanisms: surface complexation and electrostatic attraction are involved in the adsorption of As(V) (**Fig.7**) (Li et al., 2017). pH_{ZPC} of FeFPBC was found 3.045. The pH of the adsorbents is key factor in electrostatic attraction process, which depends on speciation of adsorbate and adsorbent surface charge. Due to the acidic ($FeCl_3$) treatment, more H^+ ions are available on biochar's surface. Through the electrostatic attraction process, negatively charged As(V) species adsorbed onto the positively charged biochar surface (Yoon et al., 2023). Presence of several functional groups (-OH, C-O, C=O, -CH) on the biochar's surface play a crucial role in defining the mechanism of adsorption process (Xu et al., 2023). In the FTIR analysis, it was found that biochar surface was rich in hydroxyl groups, carboxyl groups and oxygenated functional groups which helps in As(V) removal via complexation on FeFPBC surface. FTIR spectrum of the FeFPBC shows the availability of oxides of iron. Before adsorption, peak of Fe-O observed at 501.56 cm^{-1} and after adsorption it shifted at 492.24 cm^{-1} and obtained a new peak of As-O at 671.34 cm^{-1} (wang et al., 2015; Sahu et al., 2021). The obtained As peak confirmed that As(V) adsorbed on to biochar surface due to the coordinative bonding on the surface of FeFPBC. Before and after As(V) adsorption, variation of peaks intensity and shifting of peaks indicates the contribution of functional groups in possible As(V) removal mechanism.

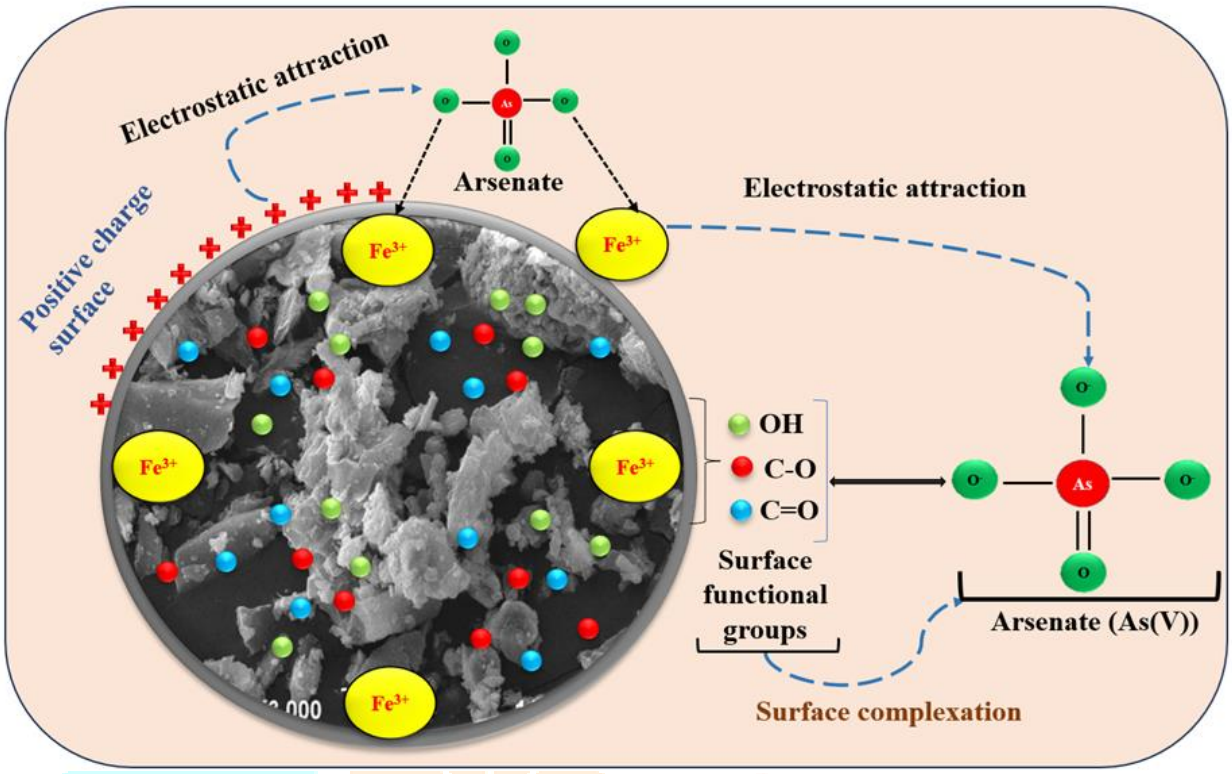

Fig.7. Mechanism for As(V) removal

3.8. Regeneration Study

The regeneration performance of the prepared FeFPBC for As(V) removal was analyzed through repeated adsorption-desorption cycles to evaluate their stability and reusability. Regeneration using 0.2 M solution of NaOH suitable for efficient desorption of As(V). **Fig.8** shows that the FeFPBC can be reused effectively for up to five cycles of As(V) removal. The study showed that biochar achieved an As(V) removal efficiency of 70.25% in the first cycle, which gradually decreased in subsequent cycles to 63.24%, 56.28%, 46.54%, and 40.72%, respectively. These results indicate that biochar can be effectively reused for as many as five cycles for the removal of As(V) from aqueous solutions.

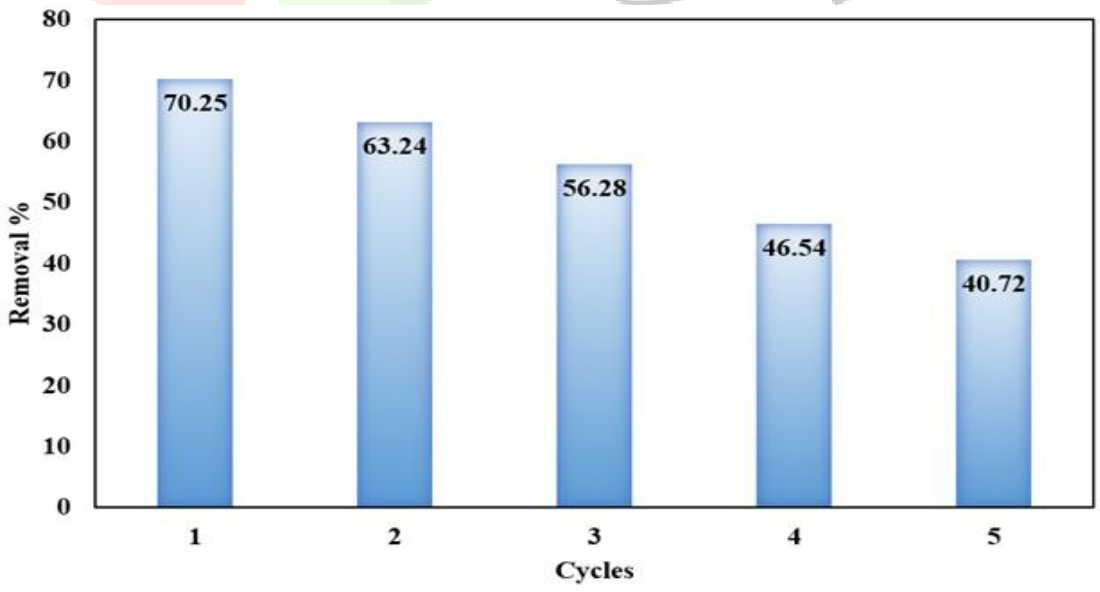

Fig.8. Regeneration study

4. Conclusion

The present study examined the adsorption efficiency of synthesized biochar (FeFPBC) for As(V) adsorption. Prepared biochar was characterized via several analysis techniques. SEM and EDS results showed that biochar's surface is rough, irregular in shape and carbon rich. FTIR results suggested that various carboxylic groups and oxygenated functional groups were present on the surface of biochar which may be helpful in As(V) adsorption process. The dose study revealed that, as the biochar dosage increased, the adsorption of As(V) also increased. Highest removal was found at 3g/L and after further dose of biochar increased, As(V) adsorption was not significantly increased. The effect of pH study showed that in the basic pH range (7 to 10 pH) removal efficiency of As(V) slightly decreased. It was found that as As(V) concentration increases, removal efficiency of As(V) decreases due to the increasing the adsorbate molecules at a specific adsorbent dose. The As (V) adsorption process was best described by the FI (R^2 = 0.9921) and the PSO kinetic model (R^2 = 0.9934), indicating heterogeneous surface adsorption and chemisorption as the dominant mechanism. The temperature study suggested that adsorption process was endothermic in nature. The above results concluded that the prepared biochar (FeFPBC) are cost-effective, reusable, efficient, and environmentally friendly for the remediation of A(V) from aqueous solution.

Reference

1. Bhan, C., Singh, J., Sahu, N., & Koduru, J. R. (2023). Reutilization of carbon of waste filter cartridge after its surface modification for the fluoride removal from water by continuous flow process. Environmental Science and Pollution Research, 30(37), 87483-87499. https://doi.org/10.1007/s11356-023-28573-y
2. Bhan, C., Singh, J., Sharma, Y. C., & Koduru, J. R. (2022). Synthesis of lanthanum-modified clay soil-based adsorbent for the fluoride removal from an aqueous solution and groundwater through batch and column process: mechanism and kinetics. Environmental Earth Sciences, 81(9), 253. https://doi.org/10.1007/s12665-022-10377-x
3. Bishnoi, S., Kumar, A., & Selvaraj, R. (2018). Facile synthesis of magnetic iron oxide nanoparticles using inedible Cynometra ramiflora fruit extract waste and their photocatalytic degradation of methylene blue dye. Materials Research Bulletin, 97, 121-127. 10.1016/j.materresbull.2017.08.040
4. Chen, Y.Y., Wang, B.Y., Xin, J., Sun, P., Wu, D., 2018. Adsorption behavior and mechanism of Cr(VI) by modified biochar derived from Enteromorpha prolifera. Ecotoxicol. Environ. Saf. 164, 440–447. https://doi.org/10.1016/j.ecoenv.2018.08.024
5. Daneshvar, M., & Hosseini, M. R. (2018). Kinetics, isotherm, and optimization of the hexavalent chromium removal from aqueous solution by a magnetic nanobiosorbent. Environ. Sci. Pollut. Res., 25, 28654-28666. https://doi.org/10.1007/s11356-018-2878-1.
6. Dong, Y., Guan, X., & Lin, H. (2026). Biochar for simultaneous soil remediation and carbon sequestration: application, mechanism, and development prospect–a comprehensive review. Environmental Earth Sciences, 85(4), 98. https://doi.org/10.1007/s12665-026-12834-3
7. Elhamdy, W.A. Environmental sustainable ZrO_2 -phosphorous Biochar nano composite derived from sugarcane bagasse and their adsorption behavior of antidepressant drugs. *BMC Chemistry* **19**, 68 (2025). https://doi.org/10.1186/s13065-025-01430-4
8. Gautam, A., Rawat, S., Verma, L., Singh, J., Sikarwar, S., Yadav, B. C., & Kalamdhad, A. S. (2018). Green synthesis of iron nanoparticle from extract of waste tea: An application for phenol red removal from aqueous solution. Environmental nanotechnology, monitoring & management, 10, 377-387. https://doi.org/10.1016/j.enmm.2018.08.003
9. Genchi, G., Lauria, G., Catalano, A., Carocci, A., & Sinicropi, M. S. (2022). Arsenic: a review on a great health issue worldwide. Applied Sciences, 12(12),6184. https://doi.org/10.3390/app12126184

10. Ibrahim, M., Siddique, A., Verma, L., Singh, J., & Koduru, J. R. (2019). Adsorptive Removal of Fluoride from Aqueous Solution by Biogenic Iron Permeated Activated Carbon Derived from Sweet Lime Waste. Acta Chimica Slovenica, 66(1).

11. Kahmann, A., Anzanello, M. J., Fogliatto, F. S., Chaovalitwongse, W. A., Marcelo, M. C. A., Ferrão, M. F., ... & Mariotti, K. C. (2018). Interval importance index to select relevant ATR-FTIR wavenumber intervals for falsified drug classification. Journal of Pharmaceutical and Biomedical Analysis, 158, 494-503.

12. Khan, S. S., & Flora, S. J. S. (2023). Arsenic: Chemistry, occurrence, and exposure. In Handbook of arsenic toxicology (pp. 1-49). Academic Press. https://doi.org/10.1016/B978-0-323-89847-8.00024-9

13. Kundu, S., & Naskar, M. K. (2021). Perspective of membrane processes for the removal of arsenic from water: an overview. Transactions of the Indian Ceramic Society, 80(1), 28-40. https://doi.org/10.1080/0371750X.2020.1864665

14. Li, H., Dong, X., da Silva, E. B., de Oliveira, L. M., Chen, Y., & Ma, L. Q. (2017). Mechanisms of metal sorption by biochars: Biochar characteristics and modifications. *Chemosphere*, *178*, 466-478. https://doi.org/10.1016/j.chemosphere.2017.03.072

15. Maji, S., Dwivedi, D. H., Singh, N., Kishor, S., & Gond, M. (2020). Agricultural waste: Its impact on environment and management approaches. In Emerging eco-friendly green technologies for wastewater treatment (pp. 329-351). Singapore: Springer Singapore. https://doi.org/10.1007/978-981-15-1390-9_15

16. Majumder, B., Sil, P., & Biswas, A. K. (2023). Arsenic Toxicity and Tolerance in Plants: Insights from Omics Studies. Heavy Metal Toxicity and Tolerance in Plants: A Biological, Omics, and Genetic Engineering Approach, 293-321. https://doi.org/10.1002/9781119906506.ch14

17. Marghade, D., Mehta, G., Shelare, S., Jadhav, G., & Nikam, K. C. (2023). Arsenic contamination in Indian groundwater: from origin to mitigation approaches for a sustainable future. Water, 15(23), 4125. https://doi.org/10.3390/w15234125

18. Mukhambet, Y., Shah, D., Tatkeyeva, G., & Sarbassov, Y. (2022). Slow pyrolysis of flax straw biomass produced in Kazakhstan: Characterization of enhanced tar and high-quality biochar. Fuel, 324, 124676. https://doi.org/10.1016/j.fuel.2022.124676

19. Muzaffar, S., Khan, J., Srivastava, R., Gorbatyuk, M. S., & Athar, M. (2023). Mechanistic understanding of the toxic effects of arsenic and warfare arsenicals on human health and environment. Cell Biology and Toxicology, 39(1), 85-110. https://doi.org/10.1007/s10565-022-09710-8

20. Natasha, Shahid, M., Imran, M., Khalid, S., Murtaza, B., Niazi, N. K., ... & Hussain, I. (2019). Arsenic environmental contamination status in South Asia. In Arsenic in drinking water and food (pp. 13-39). Singapore: Springer Singapore. https://doi.org/10.1007/978-981-13-8587-2_2

21. Peng, X., Jiang, Y., Chen, Z., Osman, A. I., Farghali, M., Rooney, D. W., & Yap, P. S. (2023). Recycling municipal, agricultural and industrial waste into energy, fertilizers, food and construction materials, and economic feasibility: a review. Environmental Chemistry Letters, 21(2), 765-801. https://doi.org/10.1007/s10311-022-01551-5

22. Rahidul Hassan, H. (2023). A review on different arsenic removal techniques used for decontamination of drinking water. Environmental Pollutants and Bioavailability, 35(1), 2165964.

23. Rashid, R., Shafiq, I., Akhter, P., Iqbal, M. J., & Hussain, M. (2021). A state-of-the-art review on wastewater treatment techniques: the effectiveness of adsorption method. Environmental Science and Pollution Research, 28(8), 9050-9066. https://doi.org/10.1007/s11356-021-12395-x

24. Rathod, S. V., Saras, P., & Gondaliya, S. M. (2024). Environmental pollution: Threats and challenges for management. In Eco-restoration of polluted environment (pp. 1-34). CRC Press.

25. Rawat, S., & Singh, J. (2021). Green synthesis of iron nanoparticles using Plumeria and Jatropha: characterization and investigation of their adsorption, regeneration and catalytic degradation efficiencies. BioNanoScience, 11(4), 1142-1153.

26. Rawat, S., & Singh, J. (2023). Fenton like oxidative degradation of toxic water pollutants by iron nanoparticles synthesized via facile green route using waste iron rust as the iron precursor. Environmental Engineering Research, 28(2).

27. Sahu, N., Singh, J., & Koduru, J. R. (2021). Removal of arsenic from aqueous solution by novel iron and iron–zirconium modified activated carbon derived from chemical carbonization of Tectona grandis sawdust: Isotherm, kinetic, thermodynamic and breakthrough curve modelling. Environmental Research, 200, 111431.

28. Sahu, N., Singh, J., & Koduru, J. R. (2021). Removal of arsenic from aqueous solution by novel iron and iron–zirconium modified activated carbon derived from chemical carbonization of Tectona grandis sawdust: Isotherm, kinetic, thermodynamic and breakthrough curve modelling. Environmental Research, 200, 111431. https://doi.org/10.1016/j.envres.2021.111431

29. Siddique, A., Nayak, A. K., & Singh, J. (2020). Synthesis of FeCl3-activated carbon derived from waste Citrus limetta peels for removal of fluoride: An eco-friendly approach for the treatment of groundwater and bio-waste collectively. Groundwater for sustainable development, 10, 100339. 10.1016/j.gsd.2020.100339

30. Siddique, A., Nayak, A. K., & Singh, J. (2020). Synthesis of FeCl3-activated carbon derived from waste Citrus limetta peels for removal of fluoride: An eco-friendly approach for the treatment of groundwater and bio-waste collectively. Groundwater for sustainable development, 10, 100339. 10.1016/j.gsd.2020.100339

31. Verma, L., Azad, A., & Singh, J. (2022). Performance of a novel iron infused biochar developed from Raphanus sativus and Artocarpus heterophyllus refuse for trivalent and pentavalent arsenic adsorption from an aqueous solution: mechanism, isotherm and kinetics study. International Journal of Phytoremediation, 24(9), 919-932. https://doi.org/10.1080/15226514.2021.1985078

32. Verma, L., Azad, A., & Singh, J. (2022). Performance of a novel iron infused biochar developed from Raphanus sativus and Artocarpus heterophyllus refuse for trivalent and pentavalent arsenic adsorption from an aqueous solution: mechanism, isotherm and kinetics study. International Journal of Phytoremediation, 24(9), 919-932. https://doi.org/10.1080/15226514.2021.1985078

33. Verma, L., Azad, A., & Singh, J. (2022). Performance of a novel iron infused biochar developed from Raphanus sativus and Artocarpus heterophyllus refuse for trivalent and pentavalent arsenic adsorption from an aqueous solution: mechanism, isotherm and kinetics study. International Journal of Phytoremediation, 24(9), 919-932. https://doi.org/10.1080/15226514.2021.1985078

34. Verma, L., Siddique, M. A., Singh, J., & Bharagava, R. N. (2019). As (III) and As (V) removal by using iron impregnated biosorbents derived from waste biomass of Citrus limmeta (peel and pulp) from the aqueous solution and ground water. Journal of environmental management, 250, 109452. https://doi.org/10.1016/j.jenvman.2019.109452

35. Verma, L., Singh, J., 2019. Synthesis of novel biochar from waste plant litter biomass for the removal of arsenic(III and V) from aqueous solution: a mechanism characterization, kinetics and thermodynamics. J. Environ. Manag. 248, 109235. https://doi.org/10.1016/j.jenvman.2019.07.006.

36. Vigdorowitsch, M., Pchelintsev, A., Tsygankova, L., & Tanygina, E. (2021). Freundlich isotherm: An adsorption model complete framework. Applied sciences, 11(17), 8078. **https://doi.org/10.3390/app11178078**

37. Wen, E., Yang, X., Chen, H., Shaheen, S. M., Sarkar, B., Xu, S., ... & Wang, H. (2021). Iron-modified biochar and water management regime-induced changes in plant growth, enzyme activities, and phytoavailability of arsenic, cadmium and lead in a paddy soil. Journal of hazardous materials, 407, 124344.

38. Wu, S., He, M., Yang, M., Zhang, B., Wang, F., & Li, Q. (2021). Near-infrared spectroscopy study of serpentine minerals and assignment of the OH group. Crystals, 11(9), 1130. **https://doi.org/10.3390/cryst11091130**

39. Xu, M., Qin, Y., Huang, Q., Beiyuan, J., Li, H., Chen, W., ... & Wang, H. (2023). Arsenic adsorption by different Fe-enriched biochars conditioned with sulfuric acid. *Environmental Science and Pollution Research*, *30*(6), 16398-16407. https://doi.org/10.1007/s11356-022-23123-4

40. Yoon, K., Cho, D. W., Kwon, G., Rinklebe, J., Wang, H., & Song, H. (2023). Practical approach of As (V) adsorption by fabricating biochar with low basicity from FeCl3 and lignin. *Chemosphere*, *329*, 138665. https://doi.org/10.1016/j.chemosphere.2023.138665